https://doi.org/10.1016/j.jcsr.2017.06.030

Strength and behaviour of reinforced double-coped beams against local web buckling

Angus C. C. Lam[b], Michael C. H. Yam[c], Cheng Fang[a]*

[a)] *Department of Structural Engineering, School of Civil Engineering, Tongji University, Shanghai 200092, China*

[b)] *Department of Civil & Environmental Engineering, University of Macau, Macau SAR, China*

[c)] *Department of Building & Real Estate, The Hong Kong Polytechnic University, Hung Hom, Kowloon, Hong Kong SAR, China*

**Corresponding author: email: chengfang@tongji.edu.cn, Tel: +86 21 65982926*

Abstract: Double-coped beams are usually employed to avoid spatial interference when similar elevations of both the top and bottom flanges of the connected beams are required. Due to the removal of the flange parts, the load resistance can be significantly compromised. This paper discusses the effectiveness of various reinforcing strategies aiming to increase the load resistance of newly designed double-coped beams or to upgrade the existing ones. A series of full-scale tests are conducted first, covering a set of reinforcement types and varying coping dimensions. Local web buckling is found to be the governing failure mode for the unreinforced specimens, and the presence of the considered stiffeners can effectively increase the load resistance. In particular, a pair of longitudinal stiffeners for the top cope edge is shown to completely mitigate the risk of local web buckling, and the final failure mode is tensile cracking at the bottom cope corner. The doubler plates, either full-depth or partial-depth, can delay the initiation of local web bucking, and as a result the load resistance is remarkably increased. The effects of the varying reinforcement types and coping dimensions on the utilisation efficiency of section capacities are discussed in detail. A finite element study is subsequently conducted to enable further understanding of key structural characteristics and to help explain some test phenomena. Preliminary design comments and recommendations are finally proposed based on the exiting test and numerical data.

Keywords: Double-coped beams (DCBs); local web buckling (LWB); reinforced; full-scale tests; numerical study.

Notation

c	coped length
D	beam depth
d_c	cope depth
L_{Rx}	extension of the stiffener or doubler plate
$M_{AISC,co}$	design moment capacity of coped section based on AISC (2010)
$M_{max\text{-}co}$	test maximum bending moment of the beam specimen at the end-of-cope section
$M_{max\text{-}p}$	test maximum bending moment of the beam specimen at the loading position
$M_{el,co}$	yield moment capacity of coped section, either with or without stiffeners
$M_{pl,b}$	plastic moment capacity of uncoped full beam section
$M_{pl,co}$	plastic moment capacity of coped section, either with or without stiffeners
M_u	coped end moment at ultimate applied load
P	applied load
P_u	ultimate applied load
R	coped end reaction
R_f	far end reaction
R_u	ultimate coped end reaction
R_{vy}	shear capacity of coped beam section
R_{wb}	elastic local web buckling capacity of DCBs without stiffeners, according to Cheng's method [16]
t_d	doubler plate thickness
t_f	flange thickness
t_w	web thickness
δ_u	in-plane deflection at ultimate load

1. Introduction

In steel structures, a similar elevation is often required for the flanges of the secondary beams (stringers) and the primary beams (girders) to satisfy architectural and construction purposes at member intersections. To achieve this, the secondary beams are usually coped at one or both flanges, as illustrated in Fig. 1(a), to avoid interference of the connected structural members, so that sufficient clearance can be provided. From the perspective of structural resistance, however, the load capacities of coped beams can be substantially decreased due to the influence of the coped region. A commonly found failure mode for a coped beam is local web buckling (LWB) [1-4]. In addition, block shear [5-9] and fatigue failures [10-12] of coped beams have also been observed and studied. The basic mechanisms and design solutions of the various local failure modes were comprehensively reviewed by Yam et al. [13]. Lateral-torsional buckling, a global buckling mode,

could also occur for coped beams if insufficient lateral restraint is applied along the compressive flange [14-15].

In order to increase the load resistance of coped beams, especially with the aim of improving the LWB performance, various reinforcing strategies have been proposed for single (compressive) flange coped beams (SCBs), as typically shown in Fig. 1(b). A numerical study on SCBs with three types of web stiffener, namely, longitudinal web stiffener (Type A), combined longitudinal and transverse web stiffeners (Type B), and doubler plate (Type C), was first conducted by Cheng et al. [16]. It was concluded that if the stiffeners were appropriately arranged, no reduction of strength occurred for the reinforced beams. The longitudinal stiffener reinforcement and doubler plate types were recommended for hot-rolled steel sections, and combined longitudinal and transverse stiffeners could be adopted for thin web members with $D/t_w > 60$ (D = beam depth, t_w = web thickness). Recently, the benefits of stiffeners on SCBs were further investigated by the authors and co-workers [17-18] via experimental investigations, where a total of 10 full-scale tests were conducted. It was found that for the specimens with longitudinal stiffeners only, the general failure mode was flexural yielding of the full beam section at the location of maximum bending moment followed by web crippling near the end-of-cope section (the section is defined in Fig. 1(a)). The general failure mode for the specimens with combined longitudinal and transverse stiffeners (Types B and D) consisted of flexural yielding of the full beam section at the location of maximum bending moment followed by flange local buckling near the loading position. Although different failure modes were induced by the use of various stiffener layouts, the reinforcements were found to increase the capacity of the coped beam specimens effectively. Further to the experimental work, numerical analysis and parametric studies were undertaken [19] investigating the effectiveness of reinforcement Types A, B, and D. Evident improvements to the beam resistance, due to the presence of the web stiffeners, were affirmed. In particular, coped beam sections reinforced by Types A and B were able to develop either the plastic moment capacity of the full beam section near the loading position or the shear yield capacity of the coped section. Moreover, Type D can be

effectively used for more slender beam sections such as built-up girders. Some of these reinforcement types have also been included in the design guideline [20].

The existing reinforcing strategies were stipulated based on the responses of SCBs, whereas relevant information on double-coped beams (DCBs) is very rare. DCBs are employed when similar elevations of both the top and bottom flanges of the connected beams are required. Compared with the case of SCBs, the reduction in resistance could be more significant for DCBs which are subjected to the removal of both flanges. A recent study conducted by the authors and co-workers [21-22] found that LWB was the major failure mode for unreinforced DCBs, and due to the different coping details, the LWB patterns of DCBs were found to be different from those of SCBs. The buckling capacity of DCBs was significantly decreased with increasing coped length (c) and cope depth (d_c). This suggests that appropriate reinforcing strategies are desirable when one wants to effectively increase the load resistance of newly designed DCBs or to upgrade the existing ones (i.e. structural retrofitting), and the importance of understanding the effectiveness of various possible reinforcement details for DCBs is highlighted.

Recognising the fact that the load resistance and failure mechanism of reinforced DCBs are still unclear, a series of full-scale tests are conducted in this study aiming to examine the effectiveness of adopting different reinforcement types for increasing the load resistance of DCBs. A finite element (FE) study is subsequently carried out to enable further understanding of the key structural characteristics and to help explain some test phenomena. Based on the current test and numerical data, preliminary design comments and recommendations are finally proposed.

2. Experimental programme

2.1 Test specimens

A total of eight full-scale specimens, made from UB406×140×39 steel beams, were tested in the research programme. The main parameters included cope length/depth (c/d_c) and stiffener types. Two reference coping dimensions were considered, and in order to highlight the influence of the stiffeners, relatively long copes, i.e. c = 450 mm (d_c = 25 mm) and c = 550 mm (d_c = 50 mm), were

selected. For each coping dimension, four specimens were tested, with one specimen unreinforced and the other three reinforced with different stiffener types, namely, 1) longitudinal web stiffener, 2) full-depth doubler plate, and 3) partial-depth doubler plate. The main aim of applying longitudinal web stiffeners was to prevent lateral deflection of the top cope edge where local web buckling (LWB) is normally initiated; when a doubler plate was applied, it was expected that a synchronous deformation pattern could be maintained for the web and the doubler plate, a mechanism which is in effect similar to increasing the web thickness (and thus to increase the LWB resistance).

The longitudinal web stiffeners, with 67.7 mm wide and 8.6 mm thick, were fillet welded (with a weld size of 6 mm) along the top edge of the coped web at both sides. The doubler plate (6.4 mm thick) was welded on one side of the coped web, and the doubler plate length was the same as that of the longitudinal stiffener. The extension of the stiffener or doubler plate (L_{Rx}) was 50 mm and 100 mm for C450 and C550 series specimens, respectively. For the case of partial-depth doubler plate, the plate depth was taken as half of the coped web depth. For both doubler plate types, fillet welds (with a weld size of 6 mm) were used. End-plate connections were considered for all the specimens, and double fillet welds were adopted to connect the beam end to the end-plate. The end plate and the column flange was connected via four snug-tightened M24 Grade 8.8 high-strength bolts. A 10 mm clearance existed between the end of the stiffener (or the doubler plate) and the end-plate. To allow a reasonable level of connection rotational flexibility, bolt washers were placed between the end plate and the supporting column face to form an approximately 4 mm-gap in between.

For easy reference, each specimen was assigned with a test code starting with cope length and depth, and ending with the reinforcement type (UR = unreinforced. LWS = longitudinal web stiffener, FDP = full-depth doubler plate, and PDP = partial-depth doubler plate), as detailed in Table 1. For instance, C450dc45-LWS stands for the specimen with the coping dimensions of c = 450 mm, d_c = 25mm, and is reinforced using longitudinal web stiffeners. Tension coupon tests

conforming to the ASTM A370 standard [23] were conducted to obtain the material property of the specimens, and the typical results are summarised in Table 2.

2.2 Test setup, instrumentation and test procedure

The test beams were arranged with a simply-supported condition. The coped end was supported by the reaction frame via the end-plate connection, and the far end of the beam was placed on a roller support which allowed in-plane rotation and horizontal movement. The span of the test beam was 2.4 m, and a concentrated load was applied by a hydraulic jack at a distance of 0.9 m from the coped end. This loading position was taken to ensure a large portion of the load being distributed to the coped end, whilst avoiding any local load bearing effect that might influence the failure behaviour of the coped region. 10-mm thick vertical stiffeners were employed at the loading and roller support locations. The applied load (P) and the far end reaction (R_f) were measured via two load cells, one placed under the hydraulic jack and the other one placed at the far end roller support. Utilising force and moment equilibriums in conjunction with the available load cell readings, the coped end reaction R and the coped end moment M can be easily calculated, i.e. $R = P - R_f$ and $M = P \times 0.9\text{m} - R_f \times 2.4\text{m}$. Only in-plane deformation was allowed for the test beams, and any lateral deformation mode, e.g. lateral-torsional buckling, of the test beam was prevented through a set of lateral bracings placed near the loading position and the roller support.

A series of strain gauges were used to measure the deformations of the coped region including the considered stiffeners, as shown in Fig. 2(b). Two strain gauges were applied at the flanges of the uncoped beam section to ensure that the concentrated load was correctly applied. Three sets of strain gauge rosette were employed over the end-of-cope section (section defined in Fig. 1(a)) to monitor the strain conditions along the boundary between the uncoped and coped region, and the strains at the other areas, including the longitudinal web stiffeners and the doubler plates, were also measured via additional strain gauges. The vertical displacements of the loading point and the end-of-cope section were measured by two in-plane linear variable differential transformers (LVDTs), and the lateral deformations of the coped region were also monitored by six

out-of-plane LVDTs distributed over the web panel. Any buckling or yield lines over the coped web could be detected through the cracking of whitewash. After installing all the instrumentations, the concentrated load was applied through two loading stages. At the early linear elastic stage, the load was gradually increased with load control. When inelastic load-displacement response of the test specimen started, stroke control was employed to better capture the nonlinear load-deflection response. All the relevant data were recorded by an automatic data acquisition system. Both ends of each test beam were treated with different coping and reinforcing details, and each beam end was considered as a separate test specimen. After completing the test on one coped end, the test beam was turned around and the opposite end was connected to the column for the subsequent testing.

3. Test results

3.1 General

The main test results are summarized in Table 3. Depending on the various coping details and stiffener types, the ultimate load P_u ranged between 98.7 kN and 481.9 kN. The in-plane deflection of the loading point at ultimate load (δ_u) also varied significantly, with larger δ_u being evidently observed for the specimens with longitudinal web stiffeners. The ultimate reaction R_u, ranging from 62.1 kN to 306.0 kN, was obtained based on the measured applied load and far-end support reaction, i.e. $R_u = P_u - R_{fu}$. Due to a certain level of rotational stiffness provided by the end-plate connection, the coped end moment at ultimate load, M_u, also existed and could be calculated using the static equilibrium condition of the test beams, $M_u = P_u \times 0.9\text{m} - R_{fu} \times 2.4\text{m}$. For most specimens, the coped end moment was insignificant, which was due to the presence of the gap between the end-plate and column face. For the two specimens with longitudinal web stiffeners, M_u could achieve 11.6 kNm (for specimen C450dc25-LWS), and it was believed that the increased coped end moment was due to gap closure which increased the connection rotational stiffness at late loading stages.

3.2 Failure modes

LWB was the governing failure mode for the two unreinforced specimens, as typically shown in Fig. 4(a). When buckling occurred, the top cope edge started to deflect in the out-of-plane direction. The ultimate load was achieved soon after the inception of LWB. With further increase of deflection, a clear buckling line was originated at approximately 1/4 to 1/3 length from the end-of-cope section, and was then extended from the top cope edge towards the bottom cope edge with a propagation angle of approximately 20º from the vertical line. With further development of the buckling line, the bottom cope edge also exhibited obvious lateral deflection.

The presence of the three considered stiffener types was shown to effectively mitigate the risk of LWB or delay its initiation, and as a result the load resistance was remarkably increased. The final failure modes for the reinforced specimens were dependent on the stiffener type. No LWB was developed when longitudinal web stiffeners were used (i.e. specimens C450dc25-LWS and C550dc50-LWS). During the initial loading process, the specimens generally behaved elastically. With increasing load, the specimens started to exhibit nonlinear response, and the longitudinal web stiffeners started to move laterally, as shown in Fig. 4(b). The lateral movement of the stiffeners was possibly caused by web crippling. Concurrently, a clear yield line appeared near the end of the longitudinal web stiffeners immediately below the top flange of the uncoped section, and this yield line was gradually spread towards the bottom flange, as shown in Fig. 4(c). Another yield line was subsequently developed, initiating at the bottom cope corner. The bottom cope corner, which sustained a high tensile stress level accompanied by stress concentration (due to geometrical discontinuity [24]), finally experienced cracking, as shown in Fig. 4(d). Afterwards the sustained load started to decrease.

For the specimens with the full-depth or partial depth doubler plate, LWB was still the major failure mode governing the ultimate load (Fig. 4(e)). However, compared with the case of unreinforced specimens, the in-plane deflection at ultimate load δ_u was almost doubled, indicating that the occurrence of buckling was effectively postponed. Upon LWB, the top cope edge started to deflect laterally, where the doubler plate tended to deform synchronously with the coped web. The

buckling line was propagated along a similar path to that observed in the unreinforced specimens, as shown in Fig. 4(f). When the lateral deformation was excessive, local damage was observed at the weld between the coped web and the doubler plate, as shown in Fig. 4(g). This was mainly caused by the tendency of shear slippage at the doubler plate-to-web interface, a phenomenon which is commonly found in composite systems, e.g. sandwich panels. Nevertheless, the weld fracture occurred at the stage beyond the ultimate load, and hence the LWB resistance the specimens was not affected. At late loading stages, yielding was also developed near the bottom cope (Fig. 4(h)), but no tensile fracture was triggered. For specimen C450dc25-FDP, a minor crack was observed at the top cope corner, as shown in Fig. 4(i). The unexpected fracture was possibly due to the significant local out-of-plane bending deformation concentrated near the top cope corner when excessive lateral deformation of the coped web occurred.

3.3 Load-deflection response

As shown in Fig. 5(a), the applied load vs. in-plane deflection (P-δ) responses were evidently influenced by the stiffeners. Linear load-deflection responses were generally exhibited at the beginning of the loading procedure. This was followed by the development of nonlinear responses after the load achieved approximately 80%-90% of the ultimate load. For the unreinforced specimens, the ultimate load, which was governed by LWB, was reached with a deflection of around 5 mm, and afterwards the load decreased with a moderate decreasing rate. For the cases of full-depth and partial-depth doubler plates, the inception of LWB was also signified by the drop of the load, but the ultimate load was sustained at larger deflections. When longitudinal web stiffeners were equipped, the linear part of the curve terminated at approximately δ = 11 mm and δ = 9 mm for specimens C450dc25-LWS and C550dc50-LWS, respectively, but the load kept increasing and the maximum deflection at ultimate load could achieve more than 35 mm. As mentioned previously, the nonlinear P-δ response was due to the development of yielding near both the top and bottom cope corners (but in the absence of LWB). Finally, the load started to drop after the occurrence of fracture at the bottom cope corner.

Fig. 5(b) shows the typical lateral deformation patterns of the coped web panel. It can be seen that some specimens started to exhibit minor lateral deformations after 10% of the ultimate load, and the lateral deformation pattern was quite irregular, a phenomenon which could result from the initial imperfection of the coped web region. With increasing load, insignificant lateral deformations (normally less than 3 mm) were developed prior to 80% of the ultimate load, and the response is coherent with the initial linear P-δ responses discussed above. For the unreinforced specimens and those with doubler plate, the lateral deformation of the coped web started to increase quickly when the applied load exceeded around 90% of the ultimate load, a sign of the inception of LWB. The largest value of the lateral deformation was recorded by LVDT3, and the corresponding location was quite close to the observed buckling line. For the two specimens with longitudinal web stiffeners, the increase of the lateral deformation was effectively suppressed, and the maximum lateral deformation was less than 8 mm by the end of the test. The minor lateral deformation of the coped web panel was developed together with the lateral movement of the stiffeners.

3.4 Strain gauge readings

Fig. 6(a) shows the typical longitudinal strain distributions over the end-of-cope section. The applied loads were selected such that the specimens were generally at the linear load-deflection stage. The calculated strains, excluding the possible stress concentration effect, were also included in the figures for comparison purposes. It is noted that the calculated strain values were derived based on the calculated moment at the end-of-cope section, i.e. R_f×(2.4-c)-P×(0.9-c), where c = cope length. The cross-sectional properties (e.g. second moment of area) were calculated taking account of both the coped web and the stiffener part. As can be seen in the figure, the test strain distributions agreed reasonably well with the calculated values. The discrepancies could result from initial geometrical imperfections which led to slight out-of-plane plate bending action over the coped web panel, noting that the strain gauges were applied at one side of the web plate. Apart from this, the stress concentration effect could also cause the difference between the test and calculated strains, especially for the specimens with longitudinal web stiffeners. This can be confirmed from

specimen C450dc25-LWS (as shown in Fig. 6(a)), where the test tensile strain near the bottom cope corner was evidently larger than the calculated one. It seemed that using doubler plates could reduce this stress concentration effect.

Fig. 6(b) shows the typical conditions of strain in the stiffeners. It was revealed that the longitudinal web stiffeners generally remained elastic prior to 90% of the ultimate load. After that, strain gauge T16 exhibited significant development of plastic strain whereas T17 still showed elastic strain. This implies that the yielded part of the stiffener was mainly concentrated near the end-of-cope section. The typical strain distribution over the doubler plate (specimen C550dc50-PDP) also showed that the plate generally remained elastic prior to 90% of the ultimate load. As expected, the top edge of the partial doubler plate was initially under compression (i.e. T16, T18, and T20). As the neutral axis of the reinforced coped section was above the web centre line, the bottom edge of the partial doubler plate was initially under tension (i.e. T17, T19, and T21). When local buckling occurred, the strain values changed significantly, and the strain development was then closely related to the LWB pattern.

It is worth mentioning that as there was no strain gauge directly mounted at the cope corners, the possible stress concentration effect could not be fully reflected by the current strain gauge readings. In order to better understand the strain/stress distributions of the coped web, a numerical investigation was conducted and will be discussed later in Section 5.

4. Discussion of test results

4.1 General

To more clearly illustrate the effectiveness of the stiffeners, the maximum (ultimate) bending moment at the loading position ($M_{max\text{-}p}$) and the associated maximum moment at the end-of-cope section ($M_{max\text{-}co}$) of the test beams are compared with the corresponding plastic moment capacity of the uncoped beam section ($M_{pl,b}$) and the yield or plastic moment capacities of the coped beam section ($M_{el,co}$ or $M_{pl,co}$), respectively, as detailed in Table 4. Moreover, the design section capacity according to AISC 360-10 [25] (Chapter F) is also included in the table, where flexural

yielding, lateral torsional buckling, and local buckling, are covered in the design. The reduced coped region was considered as an unbraced 'beam' (with length = c) under a linear bending moment distribution with the maximum moment at the end-of-cope section. It should be noted that the AISC specification is applicable to the cases of tee and rectangular sections, corresponding to the cases of UR, LWS, and FDP.

In Table 4, the moment capacities were obtained according to the measured material properties and geometric dimensions. For the coped beam sections, the cross-sectional properties (e.g. second moment of area) were calculated based on equivalent cross-sections including the stiffeners. In addition, the shear capacity (R_{vy}) and elastic LWB capacity (R_{wb}) of the coped beam section are also included in the table. The values of R_{vy} were obtained by $R_{vy} = f_y A_w / \sqrt{3}$, where f_y = yield strength, and A_w = shear resisting cross-sectional area including doubler plate. The values of R_{wb} were obtained employing Cheng's approach [16], as briefly introduced herein. For elastic LWB capacity of unreinforced DCBs, the critical moment M_{cr} can be predicted with a lateral-torsional plate buckling model assuming an unbraced length of c and a linearly-increased bending moment diagram:

$$M_{cr} = f_d \left(\frac{\pi}{c} \right) \sqrt{EI_y GJ} \tag{1}$$

where E = Young's modulus, $I_y = h_o t_w^3/12$, G = shear modulus, $J = h_o t_w^3/3$, and f_d = an adjustment factor taken as $f_d = 3.5 - 7.5(d_c/D)$ (key symbols can be found in Fig. 2(a)). Therefore, the ultimate elastic LWB reaction R_{wb} can be obtained by $R_{wb} = M_{cr}/c$. No design recommendation is currently available for predicting the LWB capacity of DCBs reinforced by stiffeners.

4.2 Effects of longitudinal stiffeners

As aforementioned, longitudinal stiffeners could effectively prevent the occurrence of LWB and to promote the development of flexural yielding near the end-of-cope section. For the unreinforced test beams, the maximum sustained moment at the loading position $M_{max\text{-}p}$ was only up to 32% of the plastic moment capacity of the beam ($M_{pl,b}$), but the $M_{max\text{-}p}/M_{pl,b}$ ratio could increase

to more than 80% when longitudinal stiffeners were added. This indicates that the plastic moment capacity of the full beam section could be better utilised when the double-coped region was reinforced by a pair of longitudinal stiffeners. For the end-of-cope section, the $M_{max\text{-}co}/M_{el,co}$ ratios are 0.76 and 0.84 for the two unreinforced specimens, and the corresponding R_u/R_{vy} ratio is significantly less than unity. These results show that the yield moment capacity of the end-of-cope section was not achieved at ultimate load, neither did shear yielding govern the failure mode. Therefore, it can be deduced that the unreinforced specimens generally failed by elastic LWB. In addition, the R_u/R_{wb} ratio is around 1.5 on average, suggesting that the Cheng's prediction for elastic LWB capacity of DCBs is on the conservative side. The AISC predictions are also overly conservative for the unreinforced specimens. The $M_{max\text{-}co}/M_{el,co}$ ratio significantly increases to 1.47 and 2.05 for specimens C450dc25-LWS and C550dc50-LWS, respectively, indicating that the reinforced coped sections failed by significant yielding rather than elastic LWB. The $M_{max\text{-}co}/M_{pl,co}$ ratios, being 0.84 and 1.14 for the two reinforced specimens, respectively, further show that the plastic moment capacity of the reinforced coped sections could be exceeded or closely approached.

Generally speaking, due to the addition of the longitudinal stiffeners, the load capacity (i.e. R_u) of specimens C450dc25-UR and C550dc50-UR was remarkably increased (by 165% and 286%, respectively), and it seemed that more remarkable improvement was achieved for the specimen with a longer cope. While the effectiveness of the longitudinal stiffeners was clearly seen, the resulting final failure mode was tensile cracking at the bottom cope corner, at which significant stress concentration could be induced.

4.3 Effects of doubler plates

The test results showed that the presence of either the full-depth or partial-depth doubler plate could increase the ultimate load, as can be seen in Table 4. For the case of full-depth doubler plate, the $M_{max\text{-}p}/M_{pl,b}$ ratios at the loading position for specimens C450dc25-FDP and C550dc50-FDP are 0.73 and 0.46, respectively, indicating that the plastic moment capacity of the full beam section was not fully achieved. The $M_{max\text{-}p}/M_{pl,b}$ results also showed that employing full-depth

doubler plate seemed to be less effective than adding a pair of longitudinal stiffeners. This is because that the introduction of the full-depth doubler plate, which is in effect similar to increasing the web thickness, tended to postpone, but not fully prevent, the occurrence of LWB. This can be confirmed by examining the $M_{max\text{-}co}/M_{el,co}$ ratio, which is slightly less than 1.0, indicating that the yield moment capacity of the reinforced coped section was not fully achieved (although quite close) prior to the occurrence of LWB. In fact, at ultimate load, evident yielding may have been developed at the cope corners due to stress concentration, and detailed stress conditions can be revealed by numerical analysis, as will be discussed later. Again, the R_u/R_{vy} ratio is significantly less than unity, showing that the failure mode of the reinforced specimens was not governed by shear yielding. The R_u/R_{wb} ratio, being less than 1.0, suggests that the Cheng's prediction [16] (based on the equivalent web thickness, i.e. $t_w + t_d$) overestimates the local web bucking capacity of the DCBs with thick webs. A previous study has also confirmed this finding [22]. The AISC prediction also tends to be unsafe for the case of FDP.

Table 4 also shows that, compared with the case of full-depth doubler plate, using the partial-depth doubler plate led to lower ultimate load for the C450dc25 series specimens. However, for the C550dc50 series specimens, the two types of doubler plate led to similar ultimate loads. At the end-of-cope section, the yield moment capacity of the PDP-reinforced coped sections was achieved, with the $M_{max\text{-}co}/M_{el,co}$ ratio being larger than 1.0. This is due to the fact that, with upshifting neutral axis of the reinforced coped section, the bottom edge of the coped region tended to yield early. The $M_{max\text{-}co}/M_{pl,co}$ ratios are less than 1.0, and therefore the plastic moment capacity of the reinforced coped sections was not achieved. Nevertheless, both the $M_{max\text{-}co}/M_{el,co}$ and $M_{max\text{-}co}/M_{pl,co}$ ratios of the PDP specimens are larger than those of the FDP specimens. This indicates that, from the material utilisation efficiency point of view, using partial-depth doubler plates may be more effective than using full-depth ones. This is because that LWB only initiates from the top (compressive) edge of the coped region, whereas the lower part, which is under tension, may be less critical to the LWB capacity.

4.4 Effects of coping dimensions

The cope length (c) and cope depth (d_c) are shown to evidently influence the LWB capacity (i.e. R_u) of the unreinforced DCBs. When c increased from 450 mm to 550 mm and d_c increased from 25 mm to 50 mm, R_u was reduced by 45.8%. The influence of increasing c and d_c can also be clearly reflected by the decreases of the $M_{max\text{-}p}/M_{pl,b}$, $M_{max\text{-}co}/M_{el,co}$, and $M_{max\text{-}co}/M_{pl,co}$ ratios. The decreased LWB capacity was mainly caused by the increase of the 'buckling length', accompanied by an increased level of compressive stress near the top cope corner, due to increased d_c (and thus decreased section modulus). The considered reinforcing strategies (i.e. longitudinal stiffeners and doubler plates) seemed to be more effective for the specimens with larger c and d_c values: for the C450dc25 series specimens, R_u was increased by a range between 68% and 165% when the coped region was reinforced; for the C550dc50 series specimens, the increasing rate could reach 149% to 286%. As a result, the difference of R_u between the C450dc25 and C550dc50 series specimens was significantly narrowed when they were reinforced. In general, the observations highlight the effectiveness of the considered reinforcing strategies for DCBs, especially for those with larger values of c and d_c.

5. Numerical study

5.1 Modelling strategy

Compared with the unreinforced DCBs, more complex failure modes, involving fracture, yielding, inelastic LWB, and potentially web crippling, were found for the specimens with varying types of stiffener. However, some of the key characteristics, including the stress pattern (with stress concentration effect) and detailed buckling/deformation modes of the specimens were not fully revealed in the test programme, and therefore a preliminary numerical study was conducted to enable further understanding of these behaviours and to help explain some test phenomena. The nonlinear finite element (FE) analysis programme ABAQUS [26] was used for this purpose. The main structural members/components, including the beam web, beam flange, stiffeners, and end-plate, were discretized using four-node quadrilateral shell elements with reduced integration (S4R),

and the meshing size was approximately 10 mm. All the members were 'tied' together, assuming no weld fracture [27]. It should be noted that the observed doubler plate-to-web weld damage, which occurred at very late stages, was not considered in the model. For the doubler plates, the reference plane of the shell elements was shifted by a value equal to the plate thickness, such that the single-sided attachment condition could be reasonably simulated. The boundary conditions, including the vertical supports and lateral bracings, were appropriately defined to reflect the actual test arrangement. The typical FE models are shown in Fig. 7(a).

An isotropic bilinear model with parameters based on the coupon test results was adopted for the steel material. The von Mises yield criterion was employed, and the true stress-strain responses, converted from engineering values, were used for the FE model [28]. The ductile damage model offered by ABAQUS was used to simulate the fractural behaviour of the coped beam web. The damage initiation criterion, which controls the maximum strain triggering initial damage, was defined based on the measured stress-strain response from the coupon tests. A damage evolution law was also employed to describe the rate of material stiffness degradation once damage is initiated, i.e. from the initiation of damage to complete loss of the element stiffness. For static analysis (ABAQUS standard solver), the degradation process should be reasonably slow to avoid convergence problem, and in the current model, a linear damage evolution law was considered, and an approximately 10% equivalent strain beyond the damage initiation strain was employed to allow the damage evolution. More details of the material model can be found in [29-30].

The analysis procedure was comprised of two steps: eigenvalue analysis and Riks analysis. The eigenvalue analysis was first conducted to obtain the first elastic buckling mode being considered as the initial geometric imperfection shape. This imperfection was then introduced in the Riks analysis model to trace the nonlinear response of the models. One can readily define the imperfection amplitude of any scale in the second step, and for the current study, an initial imperfection of $0.1t_w$ (t_w = web thickness) was provisionally considered. Previous studies have

shown that this level of imperfection could lead to reasonable predictions for a range of plated structures [22, 31].

5.2 FE results and discussions

As a preliminary FE study, the four C450dc25 series test specimens were selected and modelled. The comparisons of the load-deflection responses between the test results and FE predictions are given in Fig. 7(b). Good agreements are generally shown, especially in terms of the initial load ascending response and the ultimate load. Some minor discrepancies are observed for the unloading path beyond the ultimate load, but this has little influence on the interpretation of key structural responses. To examine the stress concentration effect of the coped region, Fig. 8(a) shows the typical stress distributions of the four models under a load level of approximately 60% of the ultimate load (P_u). As expected, stress concentration effect occurs near the top and bottom cope corners, and the stress pattern changes with varying reinforcing details. For the unreinforced model, the high stress area seems to be more extended along the top cope edge. This is probably due to the initial geometric imperfection configuration which increases the stress level near the affected ('pre-deformed') area. The highest stress of the whole model is 460.4 MPa, indicating that at 60% of P_u, most parts of the coped region remain elastic with some local areas experiencing very minor yielding (recall that f_y = 459.9 MPa for this model).

When the coped region is reinforced by a pair of longitudinal stiffeners (model C450dc25-LWS), higher stress levels (at 60% of P_u) are obviously observed at both cope corners. In addition, the upshifting of the neutral axis also contributes to the high stress level at the bottom cope corner. At the top cope corner, the high stress zone is mainly caused by significant local shear action of the web panel between the top beam flange and the stiffener. This high shear action also compromises the local web stability, a case which explains the web crippling potential (i.e. minor lateral rigid-body movement of the stiffener) observed during the test. On the other hand, the presence of the doubler plate has no critical influence on the stress pattern, although the high stress zones tend to be 'pushed' away from the doubler plate. This leads to higher stresses developed at the adjacent non-

directly stiffened part of the web, featuring a stress pattern 'embracing' the corners of the doubler plate. This higher stress at the web of the uncoped section could cause a secondary yield line originating from the top cope corner towards the lower part of the web, as can be confirmed from the test observation (Fig. 4(i)).

As a further demonstration of the failure mechanism, the predicted failure modes of the considered model group are shown in Fig. 8(b). It is clearly observed that for the unreinforced model, the predicted major buckling line agrees very well with the test observation. Due to the stress concentration effect, minor yielding is also developed near the top and bottom cope corners. The LWB-induced buckling line is prevented by the longitudinal stiffeners, and as shown in the figure, the failure mode of model C450dc25-LWS is featured by significant yielding over the entire end-of-cope section. This is in line with the fact that the yield moment capacity of this section is well mobilised with the $M_{max\text{-}co}/M_{el,co}$ ratio evidently larger than unity. When the full-depth or partial depth doubler plate is used, the general pattern of the major buckling line is not significantly changed, although the yielding area seems to be more extensive. In particular, a second yield line is originated near the top cope corner and developed surrounding the doubler plate towards the lower part of the web. This yield line echoes the aforementioned 'embraced' stress pattern at the corner of the doubler plate as shown in Fig. 8(a). The high stresses developed between the top edge of the doubler plate and the top beam flange may also explain the occurrence of local weld damage, as shown in Fig. 4(g). For all the models, there is minor yielding near the bolt holes due to considerable rotation of the end-plate at late loading stages.

6. Design comments

As mentioned in Section 1, various local reinforcing strategies have been proposed for single-coped beams (SCBs), but currently there is no such recommendation for DCBs. In the AISC Steel Construction Manual [20], three types of reinforcement, i.e. Types A to C as shown in Fig. 1(b), were suggested for common SCBs provided that L_{Rx} is larger than d_c (or $L_{Rx} \geq c/3$). It is also

recommended that when these reinforcement types are adopted, only normal yield checking for the coped section is required (i.e. 'yield checking rule').

According to the limited test and FE data presented in this study, it is seen that some of the existing reinforcing strategies for SCBs may also be well applicable to DCBs. Type A reinforcement (single longitudinal stiffeners) was shown to be the most effective reinforcing strategy considered in this study, and this reinforcement type is also recommended by the authors for DCBs. The existing design checking rule, i.e. normal yield checking for the coped section, can be safely applied to the DBCs reinforced by such stiffeners, but it is warned that the high tensile stress concentrated near the bottom cope corner may cause tensile cracking, an issue needs to receive future attention. Type B reinforcement (i.e. combined longitudinal and vertical stiffeners) may be unnecessary for the case of DCBs because web crippling, according to the current test data, is not a governing failure mode that directly influence the ultimate load. However, this conclusion builds on the condition that the beam flanges are effectively constrained laterally, e.g. composite flooring system, such that no significant lateral movement of the longitudinal stiffener is induced. If no effective lateral bracing is applied to the beam flange, e.g. bare steel beams, the vertical stiffener may bring remarkable benefits. Again, this needs further test evidence. Type C reinforcements (i.e. doubler plates) could also be considered for DCBs, although they were less effective than Type A reinforcement for the current test specimens. Importantly, it was found that the $M_{max\text{-}co}/M_{el,co}$ ratio is slightly less than 1.0 for specimens C450dc25-FDP and C550dc50-FDP, warning that the 'yield checking rule' may be unsafe. According to Table 4, the $M_{max\text{-}co}/M_{el,co}$ ratio ranges between 0.90 and 0.98, and therefore a reduction factor of 0.9 is preliminarily proposed for $M_{el,co}$ in the design of DCBs equipped with full-depth doubler plate. Type D reinforcement, using double vertical stiffeners, may have limited further benefit compared with Type B reinforcement, as a single vertical stiffener should normally be sufficient to prevent the web crippling effect. An additional reinforcement type, i.e. partial doubler plate, is also shown to increase the LWB capacity.

According to the $M_{max\text{-}co}/M_{el,co}$ ratios (ranging from 1.29 to 1.67), the 'yield checking rule' is safe and is generally on the conservative side.

The AISC design method could provide inconsistent predictions for the moment capacity of the end-of-cope section. In particular, for the unreinforced specimens, where the web thickness is relatively small, the AISC predictions are overly conservative; however, unsafe results are obtained for the FDP specimens which have an equivalent web thickness. The inaccuracy may be caused by the short length and relatively large depth of the coped region, where the yielding and buckling responses might not be well predicted using the beam analogy. The complex stress pattern of the coped region due to geometric discontinuity may cause further discrepancy between the test results and the AISC predictions. Considering the inconsistent results, the AISC approach is not recommended for predicting the moment capacity of the end-of-cope sections for unreinforced or reinforced DCBs.

The above design comments are based on the considered coping dimensions; for those beyond the current range, further studies are required. A detailed parametric study is currently underway, and the results will be reported in a separate paper.

7. Summary and conclusions

This paper has presented a comprehensive study on the effectiveness of various reinforcing strategies for strengthening double-coped beams (DCBs). A total of eight full-scale specimens have been examined, where two specimens were unreinforced and the remaining six were strengthened by three types of reinforcement, namely, 1) longitudinal web stiffener, 2) full-depth doubler plate, and 3) partial-depth doubler plate. The test results showed that the ultimate load P_u, ranging between 98.7 kN and 481.9 kN, was greatly affected by the reinforcement type and coping dimensions. Local web buckling (LWB) was the governing failure mode for the two unreinforced specimens, and the presence of the three considered stiffener types was shown to effectively increase the load resistance. In particular, no LWB was developed when longitudinal web stiffeners were used, and the final failure mode was tensile cracking at the bottom cope corner.

When the specimens were reinforced by a full-depth or partial depth doubler plate, the occurrence of LWB was effectively postponed, although LWB was still the major failure mode governing the ultimate load. Generally speaking, from the loading capacity point of view, employing doubler plate seemed to be less effective than adding a pair of longitudinal stiffeners. The test results showed that the plastic moment capacity of the coped sections reinforced by longitudinal web stiffeners could be well mobilised. For the cases of the full-depth doubler plate, the yield moment capacity of the reinforced coped sections was not fully achieved prior to the occurrence of LWB, but using partial-depth doubler plate could make the $M_{max\text{-}co}/M_{el,co}$ ratios larger than unity. In addition, the cope length and cope depth were shown to evidently influence the LWB capacity of the unreinforced DCBs, but this influence was significantly reduced when these DCBs were reinforced.

A subsequent finite element (FE) study was conducted to further reveal several key structural characteristics of the DCBs, and the buckling/deformation modes and stress distributions of the models were discussed in detail. Based on the available test and FE results, some preliminary design recommendations were proposed. In particular, it was deduced that using a pair of longitudinal stiffener can be sufficiently effective against LWB for the case of laterally restrained beams, e.g. beams with composite flooring systems, but combined longitudinal and vertical stiffeners may be necessary if no significant lateral movement is applied to the beam flange, e.g. bare steel beams. Doubler plates could also be considered for DCBs, although they were less effective for the current test specimens. It was also found that the yield checking rule may be slightly unsafe for DCBs strengthened by full-depth doubler plates, and therefore a reduction factor may be applied to the corresponding elastic section capacity. The yield checking rule could be adequately safe for the case of partial-depth doubler plate. Finally, it was found that the AISC approach is not suitable for predicting the moment capacity of the end-of-cope sections for unreinforced or reinforced DCBs.

8. Acknowledgements

The work described in this paper is fully supported by a grant from the Research Grants Council of the Hong Kong Special Administrative Region, China (Project No. PolyU 5288/13E). The assistance of Mr. Ka Man Tou and Yunhao Liu in conducting the tests is also gratefully acknowledged.

9. References

[1] Cheng JJR, Yura JA. Local web buckling of coped beams. Journal of Structural Engineering 1986;112(10):2314-31.

[2] Yam MCH, Lam ACC, Iu VP, Cheng JJR. The local web buckling strength of coped steel I-beam. Journal of Structural Engineering 2003;129(1):3-11.

[3] Aalberg A. Experimental and numerical parametric study on the capacity of coped beam ends. Journal of Constructional Steel Research 2015;113:146-55.

[4] Aalberg A. Design of aluminium beam ends with flange copes. Thin-Walled Structures 2015;94:593-602.

[5] Fang C, Lam ACC, Yam MCH, Seak KS. Block shear strength of coped beams with single-sided bolted connection. Journal of Constructional Steel Research 2013;86:153-66.

[6] Wei F, Yam MCH, Chung KF, Grondin GY. Tests on block shear of coped beams with a welded end connection. Journal of Constructional Steel Research 2010;66(11):1398-410.

[7] Lam ACC, Fang C, Yam MCH, Wang W, Iu VP. Block shear strength and design of coped beams with double bolt-line connections. Engineering Structures 2015;100: 293-307

[8] Franchuk CR, Driver RG, Grondin GY. Experimental investigation of block shear failure in coped steel beams. Canadian Journal of Civil Engineering 2003;30(5):871-81.

[9] Topkaya C. Finite element modeling of block shear failure in coped steel beams. Journal of Constructional Steel Research 2007;63(4):544-53.

[10] Yam MCH, Cheng JJR. Fatigue strength of coped steel beams. Journal of Structural Engineering 1990; 116(9):2447-63.

[11] Roeder CW, MacRae G, Leland A, Rospo A. Extending the fatigue life of riveted coped stringer connections. Journal of Bridge Engineering 2005;10(1):69-76.

[12] Wen H, Mahmoud H. Ultra-low cycle fatigue demand on coped beam connections under vertical excitations. 8th International Conference on Behavior of Steel Structures in Seismic Areas, Shanghai, China, 2015.

[13] Yam MCH, Fang C, Lam ACC, Cheng JJR. Local failures of coped steel beams – a state-of-the-art review. Journal of Constructional Steel Research 2014;102:217-32.

[14] Ibrahim SA, Dessouki AK, El -Sa'eed SA. Lateral buckling behavior and strengthening techniques of coped steel I-beams. Journal of Constructional Steel Research 2015;108:11-22.

[15] Lam CC, Yam MCH, Iu VP, Cheng JJR. Design for lateral torsional buckling of coped I-beams. Journal of Constructional Steel Research 2000;54:423-43.

[16] Cheng JJ, Yura JA, Johnson CP. Design and behavior of coped beams. Ferguson Structural Engineering Laboratory Report No. 84-1, Department of Civil Engineering, University of Texas at Austin, July, 1984.

[17] Yam MCH, Lam ACC, Wei F, Chung KF. The local web buckling strength of stiffened coped steel-I-beam. International Journal of Steel Structures 2007;7(2):129-38.

[18] Yam MCH, Ma HW, Lam ACC, Chung KF. Experimental study of the strength and behaviour of reinforced coped beams. Journal of Constructional Steel Research 2011;67:1749-59.

[19] Yam MCH, Chung KF. A numerical study of the strength and behaviour of reinforced coped beams. Journal of Constructional Steel Research 2013;80:224-34.

[20] American Institute of Steel Construction. Steel Construction Manual 14th Edition. One East Wacker Drive, Suite 700, Chicago, Illinois, 2011.

[21] Fang C, Yam MCH, Lam ACC, Liu YH, Chung KF. Local web buckling of double-coped steel beam connections. Journal of Constructional Steel Research 2017;128:166-78.

[22] Yam MCH, Fang C, Lam ACC. Local web buckling mechanism and practical design of double-coped beam connections. Engineering Structures 2016;125:54-69.

[23] ASTM A370, Standard test methods and definitions for mechanical testing of steel products. American Society for Testing and Material, Philadelphia, PA, 2002.

[24] Ratakonda R, Erdem I. Traditional Analytical Methods Underestimate the Stresses at Beam Copes. Structures Congress 2010:3270-6.

[25] AISC 360-10, Specification for structural steel buildings. American Institute of Steel Construction, Chicago, IL, USA, 2010.

[26] ABAQUS Analysis User's Manual. ABAQUS Standard, Version 6.12; 2012.

[27] Fang C, Yam MCH, Lam ACC, Xie LK. Cyclic performance of extended end-plate connections equipped with shape memory alloy bolts. Journal of Constructional Steel Research 2014;94:122-36.

[28] Yam MCH, Fang C, Lam ACC, Zhang YY. Numerical study and practical design of beam-to-column connections with shape memory alloys. Journal of Constructional Steel Research 2015;104,177-92.

[29] Wang W, Fang C, Qin X, Chen YY, Li L. Performance of practical beam-to-SHS column connections against progressive collapse. Engineering Structures 2016;106:332-47.

[30] Wei F, Fang C, Yam MCH, Zhang YY. Fracture behaviour and design of steel tensile connections with staggered bolt arrangements, International Journal of Steel Structures 2015;15(4):863-79.

[31] McCann F, Fang C, Gardner L, Silvestre N. Local buckling and ultimate strength of slender elliptical hollow sections in compression. Engineering Structures 2016;111:104-18.

Table

Table 1 Key dimensions of specimens– measured values

Test specimens	Cope length c (mm)	Cope depth d_c (mm)	c/D	d_c/D	Web thickness t_w (mm)	Flange thickness t_f (mm)	Stiffener or doubler plate thickness t_s or t_d (mm)
C450dc25-UR	450	24	1.131	0.060	6.12	8.19	-
C450dc25-LWS	450	26	1.131	0.065	6.19	8.32	8.29
C450dc25-FDP	450	26	1.131	0.065	6.22	8.28	6.28
C450dc25-PDP	450	26	1.131	0.065	6.13	8.00	6.18
C550dc50-UR	550	49	1.382	0.123	6.19	7.89	-
C550dc50-LWS	550	52	1.382	0.131	6.14	8.00	8.33
C550dc50-FDP	549	52	1.379	0.131	6.26	8.24	6.17
C550dc50-PDP	550	51	1.382	0.128	6.26	8.24	6.15

Table 2 Coupon test results for beam webs

Test specimens	Yield strength f_y (MPa)	Ultimate strength f_u (MPa)	Young's modulus E (GPa)	Strain at fracture ε_f (%)
C450dc25-UR	460	596	200	16.0
C450dc25-LWS	461	592	203	16.2
C450dc25-FDP	461	592	203	16.2
C450dc25-PDP	432	586	201	14.9
C550dc50-UR	475	601	202	15.4
C550dc50-LWS	432	586	201	14.9
C550dc50-FDP	434	575	197	16.5
C550dc50-PDP	434	575	197	16.5

Table 3 Summary of test results

Test specimens	Ultimate load P_u (kN)	Deflection at ultimate load δ_u (mm)	Ultimate Reaction R_u (kN)	Ultimate coped end moment M_u (kN.m)	Failure mode
C450dc25-UR	180.7	5.4	114.5	3.8	LWB
C450dc25-LWS	481.9	25.8	306.0	11.6	FCC
C450dc25-FDP	385.7	10.3	241.8	1.8	LWB
C450dc25-PDP	306.9	9.1	192.6	1.9	LWB
C550dc50-UR	98.7	5.4	62.1	1.0	LWB
C550dc50-LWS	379.1	36.9	239.8	9.1	FCC
C550dc50-FDP	244.6	9.1	155.7	6.8	LWB
C550dc50-PDP	243.9	9.8	154.4	4.7	LWB

Note: LWB = local web buckling; FCC = fracture of cope corner.

Table 4 Discussion of test results

Test specimens	R_u (kN)	$M_{max\text{-}p}$ (kNm)	$M_{max\text{-}co}$ (kNm)	$M_{pl,b}$ (kNm)	$M_{el,co}$ (kNm)	$M_{pl,co}$ (kNm)	$M_{AISC,co}$ (kNm)	R_{vy} (kN)	R_{wb} (kN)	$\frac{M_{max\text{-}p}}{M_{pl,b}}$	$\frac{M_{max\text{-}co}}{M_{el,co}}$	$\frac{M_{max\text{-}co}}{M_{pl,co}}$	$\frac{M_{max\text{-}co}}{M_{AISC,co}}$	$\frac{R_u}{R_{vy}}$	$\frac{R_u}{R_{wb}}$
C450dc25-UR	114.5	99.3	47.8	305.9	56.8	85.2	19.2	566.4	79.4	0.32	0.84	0.56	2.49	0.20	1.44
C450dc25-LWS	303.5	267.6	131.0	295.6	89.0	156.2	142.4	605.6	-	0.91	1.47	0.84	0.92	0.50	-
C450dc25-FDP	241.8	215.9	107.0	295.6	118.9	178.8	175.8*	1185.4	719.0*	0.73	0.90	0.60	0.61*	0.20	0.37*
C450dc25-PDP	192.6	171.5	84.8	253.9	65.6	114.8	-	834.0	-	0.68	1.29	0.74	-	0.23	-
C550dc50-UR	62.1	54.9	33.2	302.1	43.5	65.9	13.9	507.0	39.6	0.18	0.76	0.50	2.39	0.12	1.57
C550dc50-LWS	239.8	209.0	125.0	253.9	60.9	109.2	97.4	470.2	-	0.82	2.05	1.14	1.28	0.51	-
C550dc50-FDP	155.7	133.4	78.9	287.5	80.7	121.5	116.7*	938.6	330.3*	0.46	0.98	0.65	0.68*	0.17	0.47*
C550dc50-PDP	154.4	134.3	80.2	287.5	48.0	84.0	-	707.5	-	0.47	1.67	0.95	-	0.22	-

Note: * results are obtained based on equivalent web thickness ($t_w + t_d$)

Figure
Click here to download Figure: All figures_r2.doc

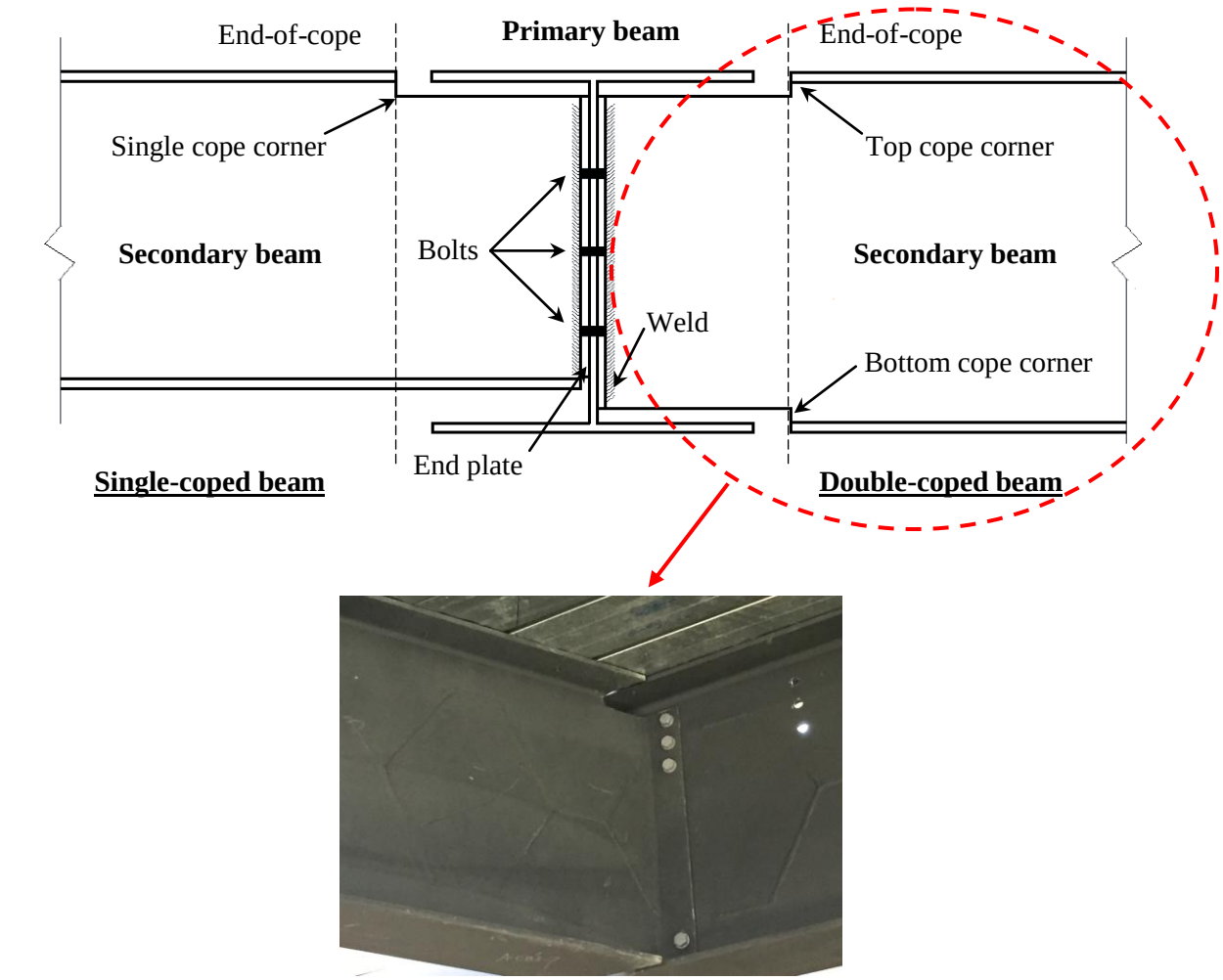

(a)

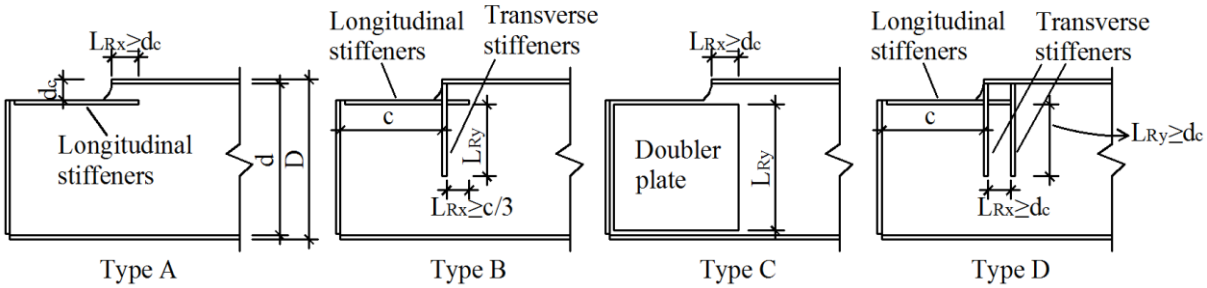

(b)

Fig. 1 Detailing of coped beams: a) practical double-coped beams (DCBs), b) typical reinforcing strategies for single-coped beams (SCBs)

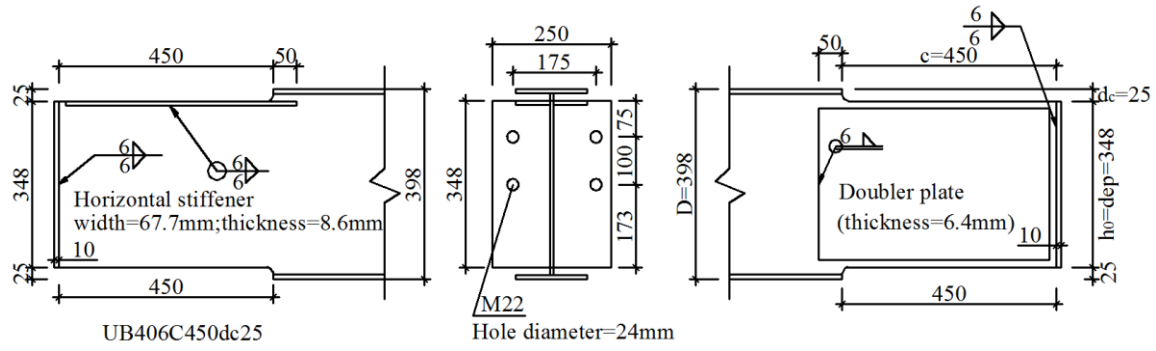

(a)

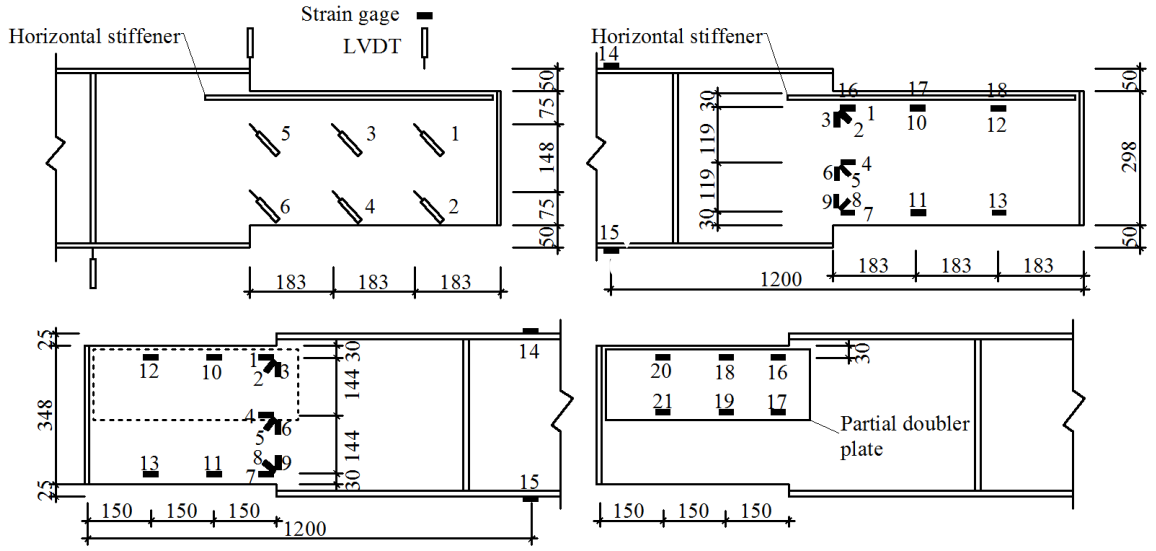

(b)

Fig. 2 Test specimens: a) specimen details and key symbols, b) instrumentations

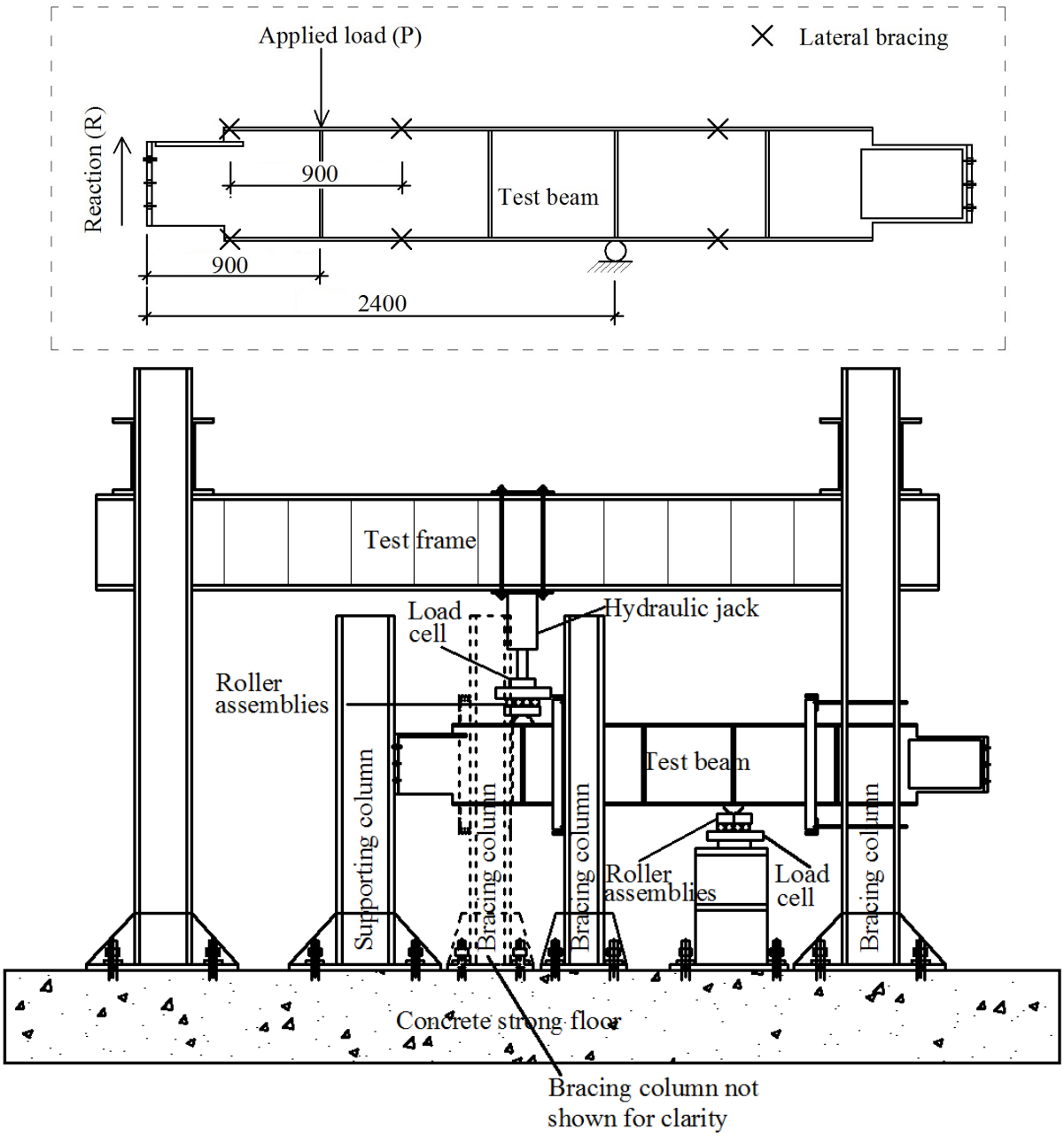

Fig. 3 Schematic illustrations of test setup

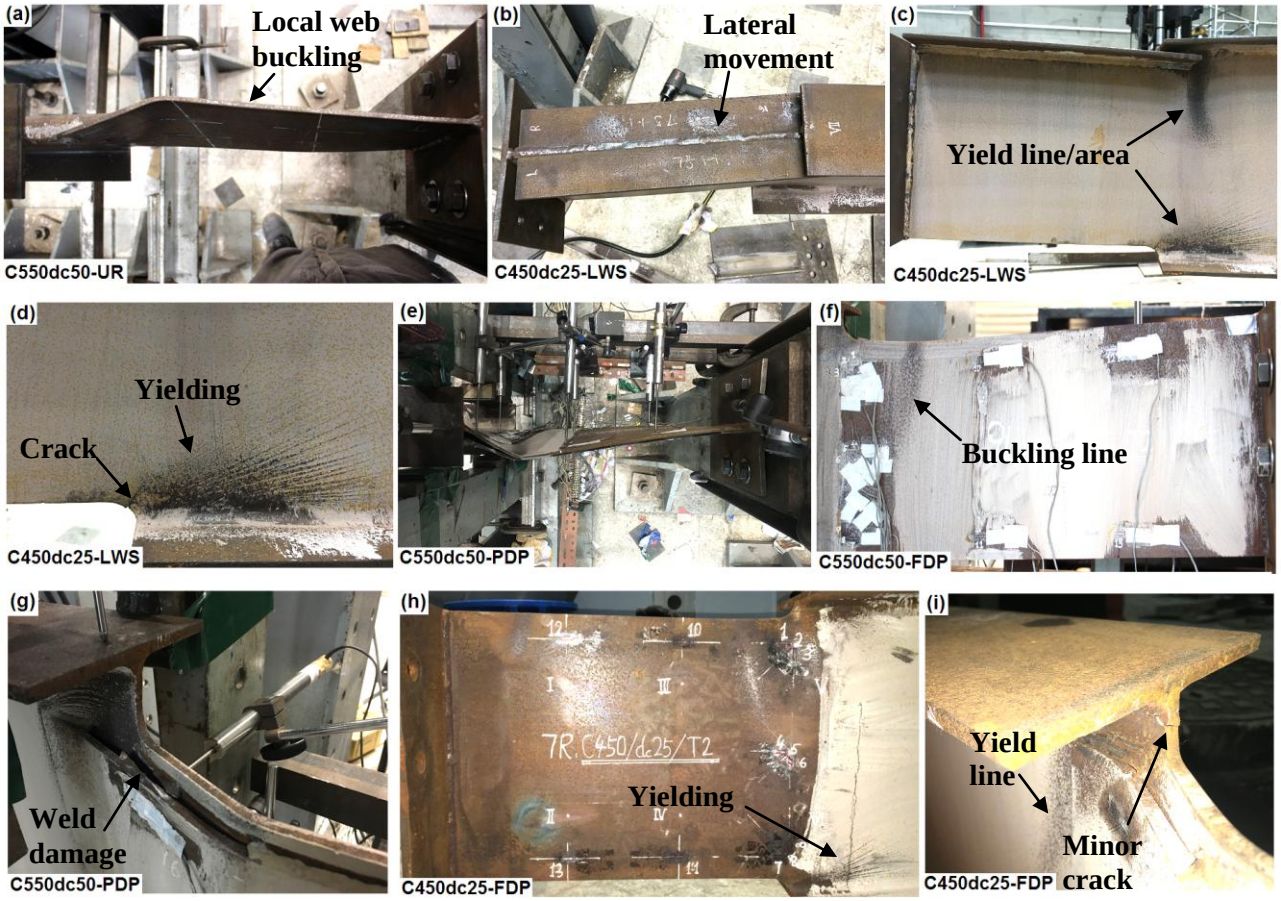

Fig. 4 Typical failure modes of specimens

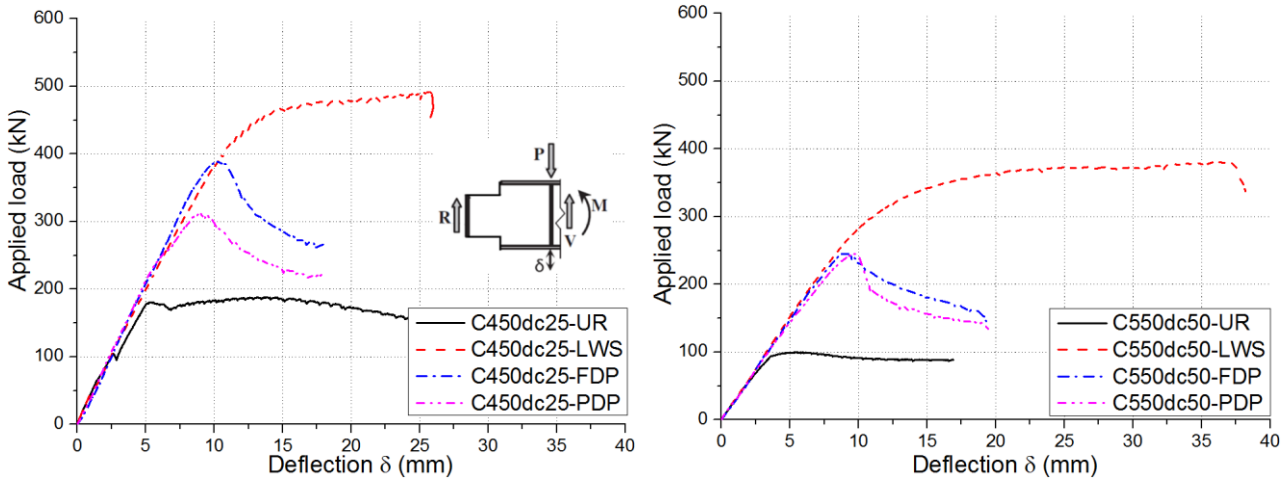

(a)

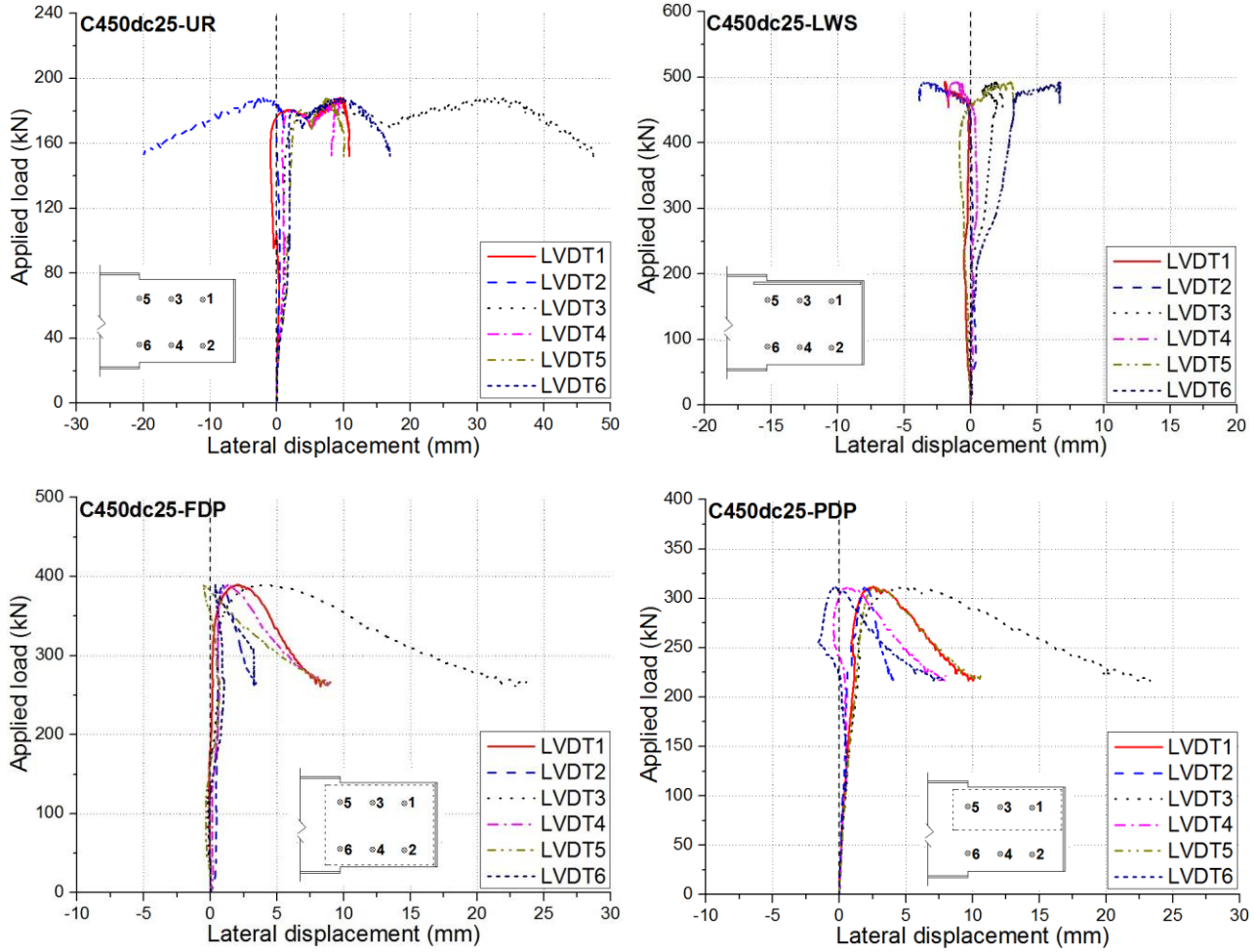

(b)

Fig. 5 Load-deformation responses: a) load-vertical deflection curves, b) load-lateral deformation curves

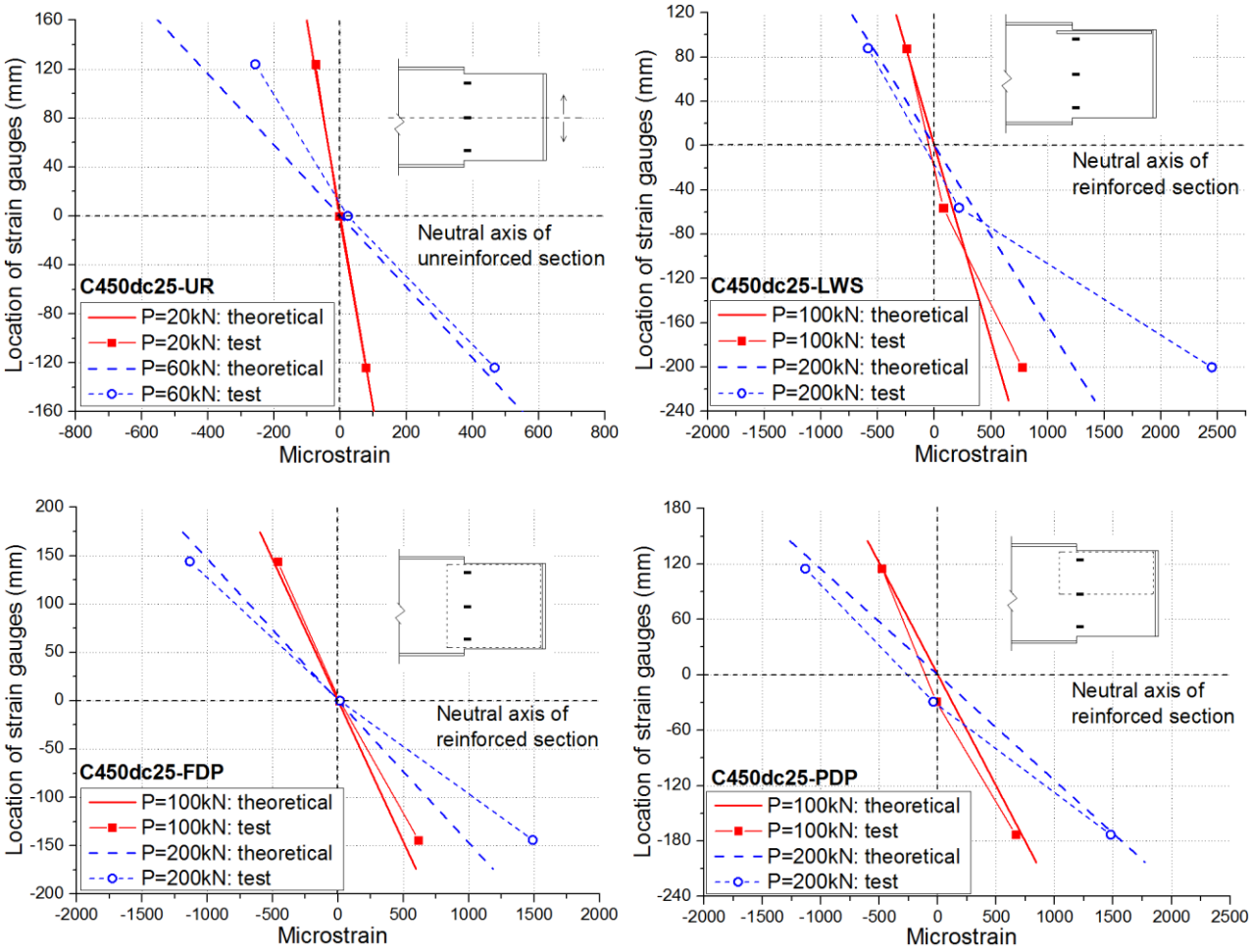

(a)

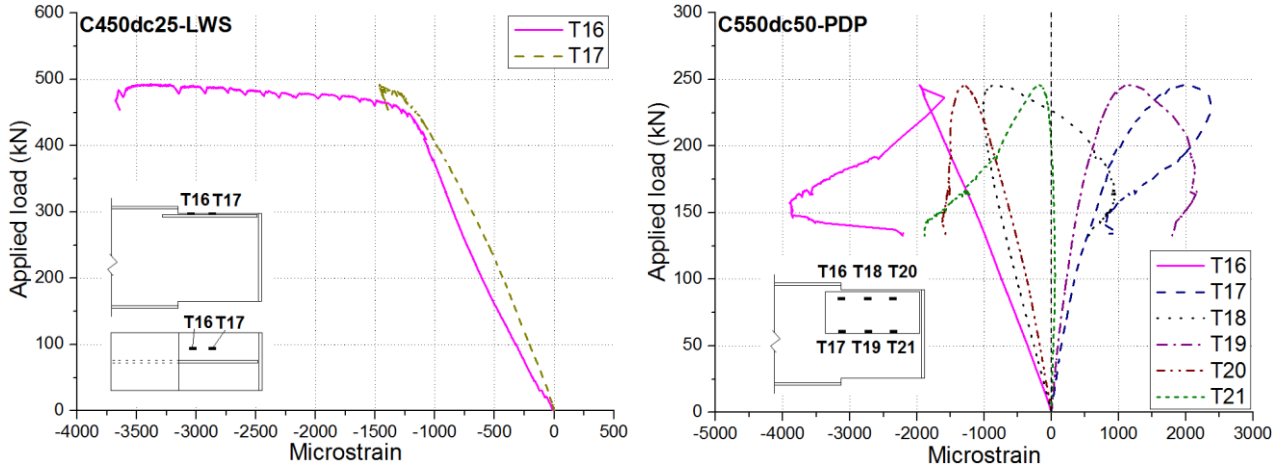

(b)

Fig. 6 Typical strain gauge readings: a) strains of beam webs, b) strains of stiffeners and doubler plates

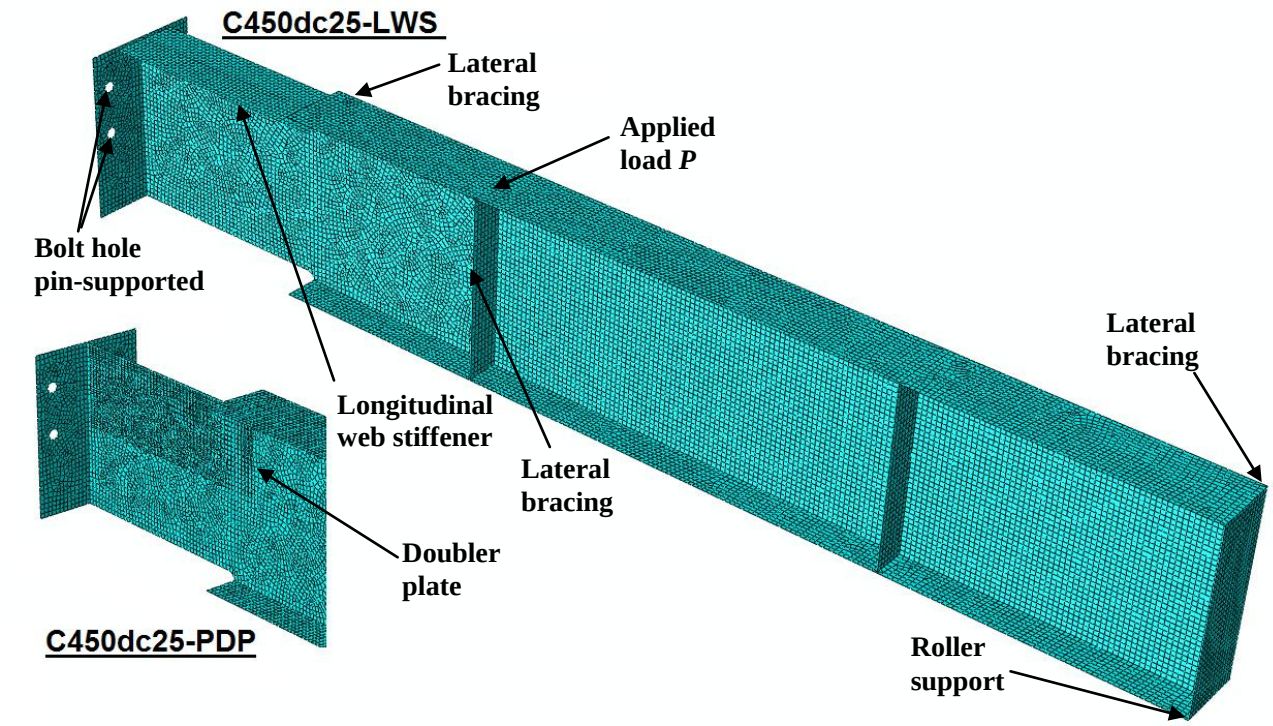

(a)

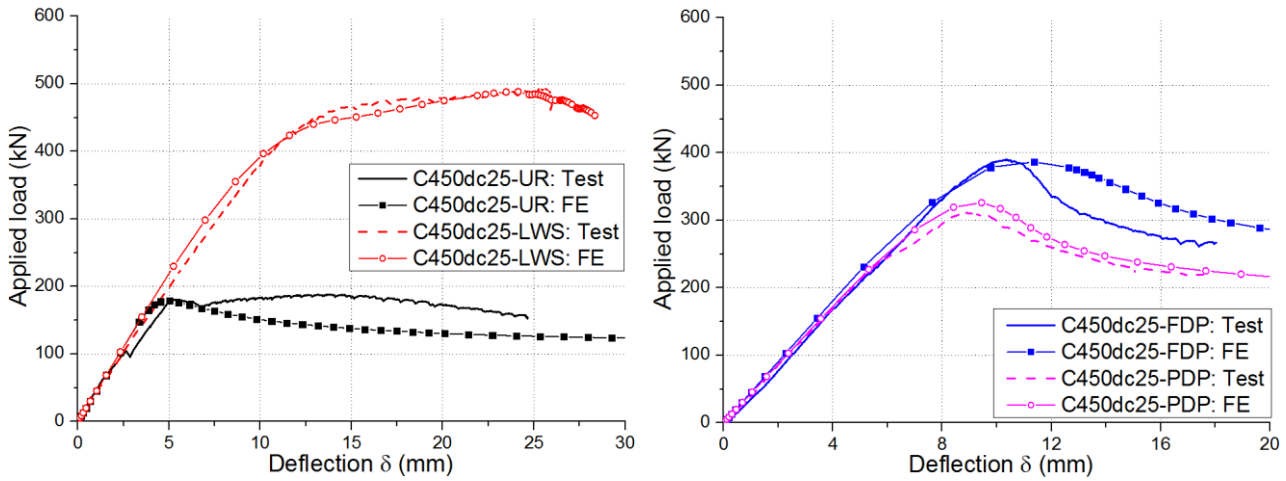

(b)

Fig. 7 FE studies: a) typical FE model and meshing scheme, b) comparisons of load-deflection responses

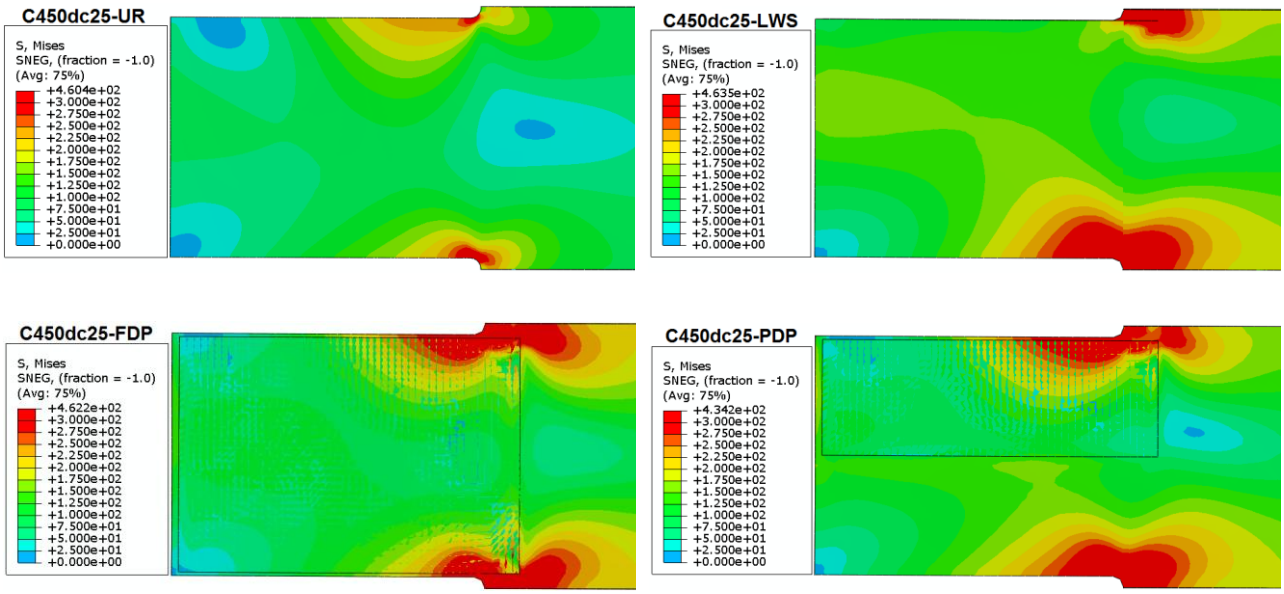

(a)

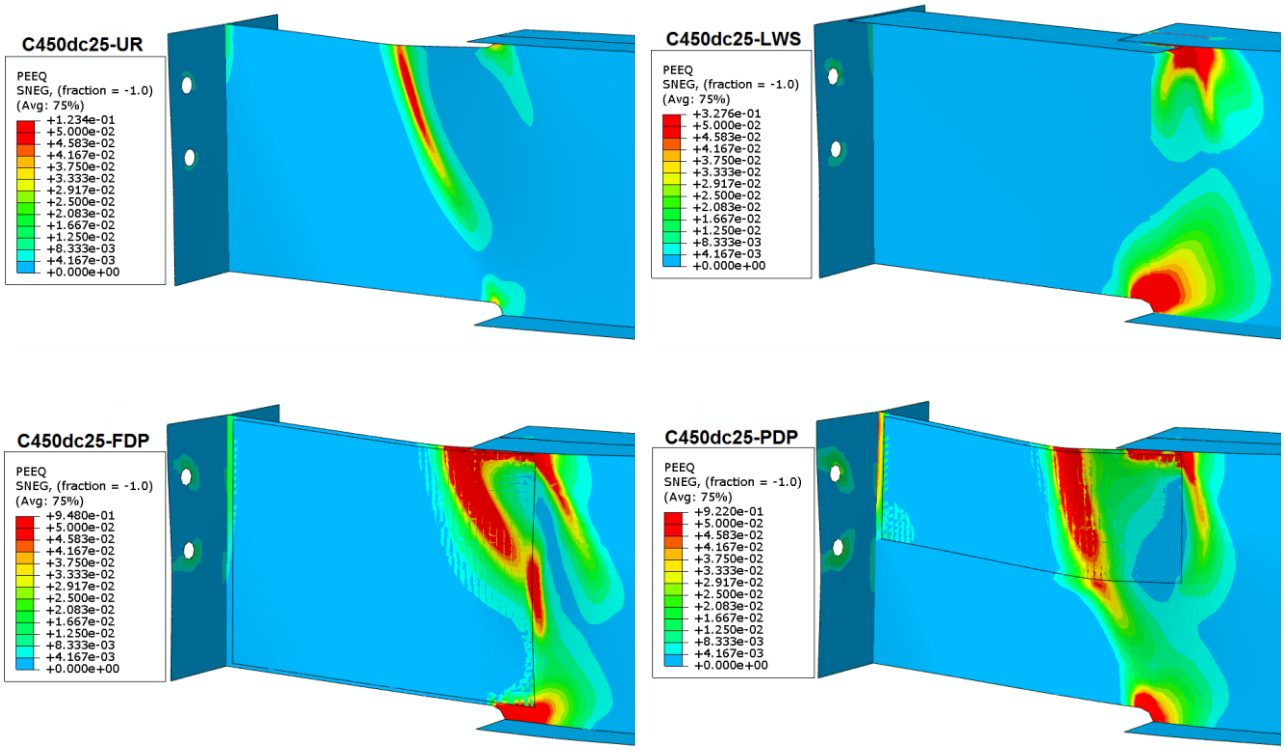

(b)

Fig. 8 Finite element predictions: a) stress distributions at 60% of ultimate load, b) final failure modes